plasma

MDPI

Article

Anodization Time Effect on Silver Particles Deposition on Anodic Oxide Coating over Al Produced by Plasma Electrolytic Oxidation

Francisco Trivinho-Strixino [1,*], Adriana O. Delgado-Silva [1], Janaina S. Santos [1], Andressa Rodrigues [1], Giovanni P. Mambrini [1] and Mariana S. Sikora [2]

[1] Department of Physics, Chemistry and Mathematics, Federal University of São Carlos (UFSCar)—Sorocaba Campus, Sorocaba 18052-780, SP, Brazil
[2] Department of Chemistry, Federal University of Technology—Paraná (UTFPR), Pato Branco 85503-390, PR, Brazil
* Correspondence: fstrixino@ufscar.br

Abstract: In this study, 6061 Al alloy was galvanostatically anodized under the Plasma Electrolytic Oxidation (PEO) condition. A factorial design of 2^2 was carried out using two variables (anodization time and presence of silver in the electrolyte) on two levels, i.e., 20 and 60 min of anodization and the absence/presence of silver ions in the electrolyte. The Al anodization was performed in sodium silicate electrolyte, applying a constant current density of 20 mA cm^{-2}. The oxide characterization was performed by Scanning Electron Microscopy (SEM), surface roughness analysis (RMS), Energy Dispersive Spectroscopy (EDS), Rutherford Backscattered Spectroscopy (RBS), and Grazing Incidence X-ray Diffraction (GIXRD). The SEM micrographs revealed an irregular porous structure with cracks on the oxide surface composed of a thin crystalline layer of γ-Al_2O_3 over the Al substrate. From EDS and RBS analysis, it was possible to identify the elements Al, O, Si, Ag, and Na, demonstrating that a shorter anodization time (20 min) led to a significant amount of silver deposits on the outer layer of the oxide coating, mainly deposited in the surroundings of the pores. Conversely, the silver content on the PEO film anodized for 60 min was meager. These results demonstrated that the anodization time was the critical control variable for the amount of silver deposited over the oxide film. The shorter the anodizing time, the higher the silver content on the PEO coating.

Keywords: Plasma Electrolytic Oxidation (PEO); aluminum anodization; silver deposition; alumina coatings

Citation: Trivinho-Strixino, F.; Delgado-Silva, A.O.; Santos, J.S.; Rodrigues, A.; Mambrini, G.P.; Sikora, M.S. Anodization Time Effect on Silver Particles Deposition on Anodic Oxide Coating over Al Produced by Plasma Electrolytic Oxidation. *Plasma* **2023**, *6*, 235–249. https://doi.org/10.3390/plasma6020018

Academic Editor: Andrey Starikovskiy

Received: 14 February 2023
Revised: 27 March 2023
Accepted: 14 April 2023
Published: 23 April 2023

1. Introduction

This study investigated the influence of anodization time for silver nanoparticles deposition over alumina coatings fabricated by Plasma Electrolytic Oxidation (PEO) on 6061 aluminum alloy (AA6061) in sodium silicate media. This technique is commonly used for surface treatment of Al, Ti, Mg, Nb, Zr, and their alloys [1–3], forming an oxide layer that is rigidly adhered to the metal substrate with high electrical and mechanical resistance. The composition, morphology, and microstructure of the anodic oxide can be controlled by experimental conditions, such as electrolyte composition, applied current or voltage, temperature, and duration, which can lead to the formation of coatings with different properties [3–5]. Different from the conventional anodization, a high applied voltage is imposed in the anode to promote the oxide dielectric breakdown, which favors the incorporation of species from the electrolyte into the oxide films due to simultaneous events occurring during PEO processes, such as localized destruction/rebuilding of oxide, electric discharges, plasma formation, gas evolution, Joule heating, and cooling [1,6,7]. Adding specific ions or particles in the electrolyte can modify the coating properties [8–11], tailoring them to a particular interest or industrial application. Additionally, this technique

is advantageous in terms of synthesis duration, allowing the fabrication of alumina coatings for different purposes in a fast one-step fabrication method.

Regarding the Aluminum PEO, reports in the literature have described the incorporation of particles into the oxide coating from the electrolyte to enhance their corrosion resistance, wear, and tribological properties [12–15], catalytic activity [16–18], magnetic properties [19,20], and antimicrobial properties [21–26]. Studies that focus on improving the corrosion resistance and tribological properties reported the use of carbon-based additives [12,13] and α-Al_2O_3 [14], and ZrO_2 [15] powders in the electrolyte. In addition, W, Co, and Ni species are reported as an additive in PEO electrolytes to improve the catalytic properties of alumina coatings in thiophene oxidation [16] and CO conversion to CO_2 [17,18]. On the other hand, Fe species were incorporated from the electrolyte to provide a magnetic property to the PEO oxide coatings [19,20]. For improving antibacterial and antifouling properties, silver [22–25] and copper [21,22,26] were explored as additives of alumina PEO coatings produced in silicate media.

The incorporation of antimicrobial agents from the electrolyte is widely explored on PEO coatings produced over Ti and Mg substrates for biomedical applications [27–32]. Still, it is not commonly employed in aluminum alloys because of the low biocompatibility of this metal. Therefore, relatively few studies using silver species to modify the anodic alumina using PEO can be found in the literature. Nevertheless, as a metal-base substrate employed in several areas, surface treatments in Al can be a strategic solution to bioburden control and healthcare environments such as hospitals [33,34]. For example, some authors demonstrated that adding silver powders in the alkaline silicate electrolytes significantly enhanced the antifouling and antibacterial properties of PEO coatings on AA7075 alloys [22–24]. On the other hand, Santos et al. [25] observed that the incorporation of silver particles or silver ions into the alumina coating and the antimicrobial effectiveness were dependent on the electrolyte design.

The present work investigated the effects of anodizing time and silver addition in the electrolyte for Al treatment by PEO. Silver nitrate salt was chosen as the silver precursor. Using powder additives directly to the electrolyte is a common strategy [8], despite increasing solution resistivity and PEO voltage, which requires more energy input. Therefore, in this study, the incorporation of silver in the ionic form was carried out to ensure the required energy during the metal treatment. The oxide was produced in one step and monitored by transient voltage curves. The characterization was performed by Scanning Electron Microscopy with Energy Dispersive Spectroscopy (SEM-EDS), Rutherford Backscattered Spectroscopy (RBS), roughness analysis (RMS), and Grazing Incidence X-ray Diffraction (GIXRD). The findings revealed an alternative to depositing silver species over the aluminum substrate using a fast one-step synthesis.

2. Experimental Procedure

Anodic oxide coatings were grown in 6061 Al alloy substrates by PEO. Samples were cut in reduced dimensions (2.0 cm $\times$ 0.5 cm $\times$ 0.6 cm), mechanically polished using #600 and #1200 sandpapers, and degreased with acetone and detergent. The PEO treatment was carried out in an electrolytic reactor with an external cooling system. Two platinum foils were used as cathodes parallel to the anode to obtain a homogeneous electric field distribution over the electrode surfaces and a total anode area of 1 cm^2 immersed in the electrolyte. Constant current anodization was performed using a Keithley 2410 1100 V Source Meter coupled to a high-potential probe (Tektronix—P6015A). A digital recorder (E-Corder 410 Edaq) acquired the potential transient curves in situ with a 40 Hz sampling rate. The samples were prepared in an alkaline aqueous solution containing 0.1 mol L^{-1} Na_2SiO_3 (conductivity 19.9 $\pm$ 1.0 $\mu S\ cm^{-2}$, pH 12.4 $\pm$ 1.0) with and without 1 mmol L^{-1} $AgNO_3$ (conductivity 20.0 $\pm$ 1.0 μScm^{-2}, pH 12.2 $\pm$ 1.0) and under magnetic bar stirring. A constant current of 20 mA cm^{-2} was applied during the experiment, and two sets of coatings were produced under two anodization time levels: 20 and 60 min. The electrolyte temperature during the synthesis was recorded, started at 25 °C before the PEO ignition,

and increased up to 29.2 ± 0.3 °C till the end of anodization. The samples prepared after PEO treatment were cleaned with distilled water and air-dried.

2.1. Material Characterization

The morphology and microstructure of PEO surface coatings were characterized by high-resolution FEG-SEM Quanta 650.

A Hitachi TM3000 Tabletop Microscope obtained the semi-quantitative composition analysis with EDS. After anodization, the surface color-map analysis was used to illustrate the Ag distribution on the alumina coating over the Al substrate.

Investigation of elemental chemical composition and depth profile was carried out using RBS measurements at the Laboratory for Material Analysis with Ion Beams (LAMFI-USP) of the University of Sao Paulo, employing ion beams of He^+ with 2.2 MeV energies in a Pelletron Tandem accelerator. Two solid-state SSB detectors were placed at scattering angles of 122° and 170°, respective to the ion beam direction. The samples were placed at an angle of −7°, respective to the normal ion incidence, and the measurements were performed with 10 μC of charge accumulation. A quantitative and self-consistent analysis of the RBS spectra was made using the MultiSIMNRA platform [35], fitting all spectra simultaneously on several instances of the SIMNRA software [36]. Minimizing an objective χ2 function, MultiSIMNRA calculates a reasonable elemental depth profile of the sample that best explains all spectra simultaneously, assuming a model with several homogenous thin layers. Duplicate samples were submitted to RBS analysis.

The crystal structure of the PEO alumina layer was investigated in Grazing Incidence X-ray Diffraction (GIXRD) mode using a Shimadzu XRD-6100 with Cu Kα radiation (λ =1.5418 Å) at 40 kV and 30 mA. The GIXRD patterns were recorded in the 2θ range of 10–90° with a 0.02° step (10 s per step) and a fixed θ value of 10°. In addition, the crystallite size of the γ-Al_2O_3 phase was determined by diffraction peak at 2θ = 66.9° and using Scherrer's equation [37]. The GIXDR analysis was performed in duplicate.

The roughness of the PEO coatings was determined using a profilometer Veeco DekTak ISO mode Standard Scan with 12.5 μm radius, 3 mg force, 2000 μm length, 0.513 μm $sample^{-1}$ resolution, and an analysis duration of 13 s. Ten measurements were performed in each sample at different surface points. All the experiments were performed in triplicate.

2.2. Factorial Design

This study used a 2^2 factorial design (2 variables and two levels), resulting in four experiments (2^2 = 4). One of the advantages of using this chemometric procedure is reducing the required number of experiments for large-scale procedures and quantifying the main and cross-linked effects of each variable in some specific responses [30,31]. Based on a previous study [25], the anodization time and the silver content in the electrolyte were chosen as variables. These variables were studied at two fixed levels indicated by (-) and (+) in the factorial design matrix in Table 1. The three different responses were analyzed. As a morphological response, the surface roughness of the oxide was measured (Root mean square—RMS). The microstructural response was the crystallite size, whereas the compositional response was the percentage of Ag and Si on the surface of the oxide layer. A 95% confidence interval was used to calculate the experimental error associated with the responses and variable effects.

Table 1. 2^2 factorial design combining experimental variables with their values and the analyzed responses.

Variable	Level (−)	Level (+)	Exp.	A	B
(A) **Anodization time (min.)**	20	60	S20	−	−
(B) **Ag^+ ion content**	Without	With	S60	+	−
Responses: RMS, Crystallite size, Ag and Si content			S20Ag	−	+
			S60Ag	+	+

3. Results and Discussion

Figure 1 depicts the transient voltage profiles of aluminum obtained under the galvanostatic regime according to the experimental conditions presented in Table 1. Two distinct regions (I and II) can be identified in the voltage transients. In region I, an almost linear increase in voltage up to about 350–400 V is observed due to the oxide barrier growth. Region II is characterized by the oscillatory voltage observed during the PEO process [3,6,38].

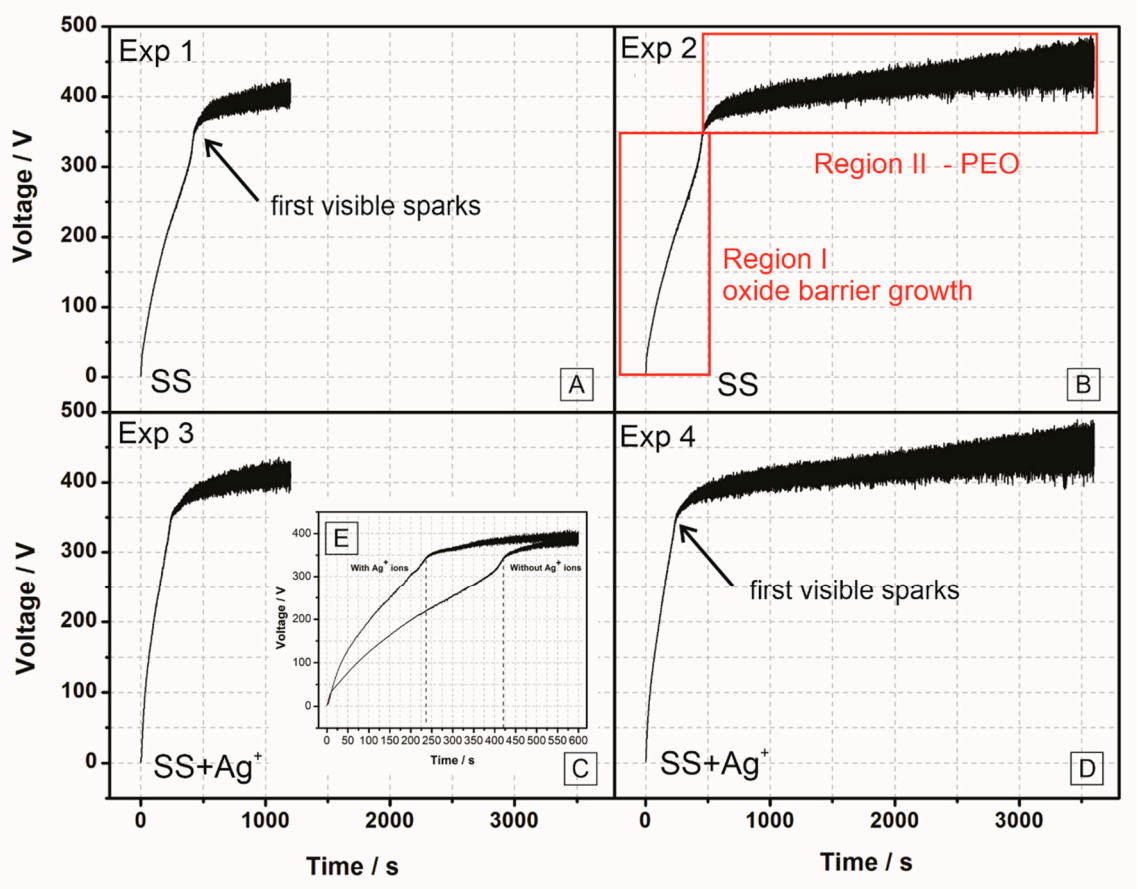

Figure 1. Voltage transient curves for Al anodization in sodium silicate solution (SS) (**A**,**B**) and sodium silicate solution containing Ag^+ ions (SS + Ag^+) (**C**–**E**) according to Table 1. Inset: early stages of the voltage transient curves indicating the beginning (vertical traced lines) of region II and the PEO ignition with sparks, with and without silver ions in the electrolyte.

The primary process responsible for oxide growth in the region I (Figure 1B) is the ionic transport and the oxide growth on the interface metal/oxide [39]. As the oxide film

thickness increases, the potential rises to maintain the electrical field constant until the oxide thickness reaches a critical value. After this stage, a transition to a more intense breakdown occurred with a voltage-transient slope change accompanied by heat, light release, gas evolution, and voltage oscillations. The second region (Figure 1B) starts with the ignition of the first sparks and the characteristic potential oscillatory behavior of the PEO process [3,4]. At the beginning of this process, it is possible to visualize the first short-lived sparks that contain a small area and low luminosity intensity and are uniformly distributed over the coating surface, as observed in other studies [6]. In addition, small amplitude fluctuations in voltage values were observed in this region and are associated with continuous oxide destruction and rebuilding processes [40]. Once the oxide film is disrupted, the reduced resistance at the exposed spot sites causes a current increase with a simultaneous voltage decrease [41]. This process is followed immediately by the rapid growth of the oxide film, which increases the voltage due to the local resistance of the oxide at such spots, resulting in oscillatory behavior. As the anodization continues, sparking discharges become more intense with longer lifetimes [4]. At this stage, the sparks grow in size and duration, turning into micro arc discharges that appeared randomly distributed over the surface coating [6,39]. A longer anodizing period applying constant current PEO led to the micro arc regime, with more destructive effects on the oxide layer. Therefore, since the anodizing time in the galvanostatic regime is correlated with the characteristics of the sparks, it also influences the coating morphology.

Furthermore, as can be seen in the inset of Figure 1E, the presence of Ag^+ ions in the electrolyte might accelerate the oxide growth process, which can be noted by the onset of the voltage oscillations where the oxide film reaches the critical thickness and the PEO process begins. The breakdown voltage was observed at ~230 s in anodization with Ag-containing electrolyte and ~420 s without silver. The effect of this time-lapse may be related to changes in oxide composition and morphology during its formation since the physicochemical properties of the electrolyte (pH and molar conductivity) do not change with the presence of Ag ions. Furthermore, the formation of insoluble particles dispersed in electrolyte solution can be observed during the experiment carried out in different anodization times and in the presence of Ag^+ ions, which might be responsible for this behavior. These particles can result from a precipitation reaction between silicate anion and Ag^+ cation at the initial stages of the anodization (Equation (1)) or a process associated with a reaction of the electrolyte ionic species in contact with the anode surface during the spark and micro-arc regimes.

$$2Ag^{+}_{(aq)} + SiO_3{}^{2-}_{(aq)} \rightarrow Ag_2SiO_{3\ (s)} \quad (1)$$

Both assumptions consider a change in silver concentration in the electrolyte and its availability to deposition over the substrate. At this moment, it is impossible to assume which of both hypotheses occurred. However, this behavior significantly influences the morphology and composition of coatings, as pointed out in the subsequent description of the results.

The properties of the oxide layer produced by PEO on aluminum depend on the experimental conditions, mainly the type of electrolyte used [25]. Figure 2 shows the SEM micrographs of alumina coatings produced under the experimental conditions depicted in Table 1. The oxide layer produced in sodium silicate and Ag-containing sodium silicate solutions showed a structure with an irregular porous distribution, with large elongated pores, tiny pores, and protrusions. As can be seen in Figure 2, SEM micrographs reveal different types of coatings, depicting small porous (~2 μm in diameter) and large porous (~5 μm in diameter) depending on experimental conditions, and "hill-like" protrusion structures on the surface [42]. From a visual inspection of the micrographs in Figure 2A,C, a high number of small pores can be seen in the experiments performed for a short anodization time, S20 and S20Ag, when compared with a longer anodization time (S60 and S60Ag) (Figure 2B,D), where more prominent protrusions and elongated porous were observed. Some of the elongated pores may originate from micropore connections.

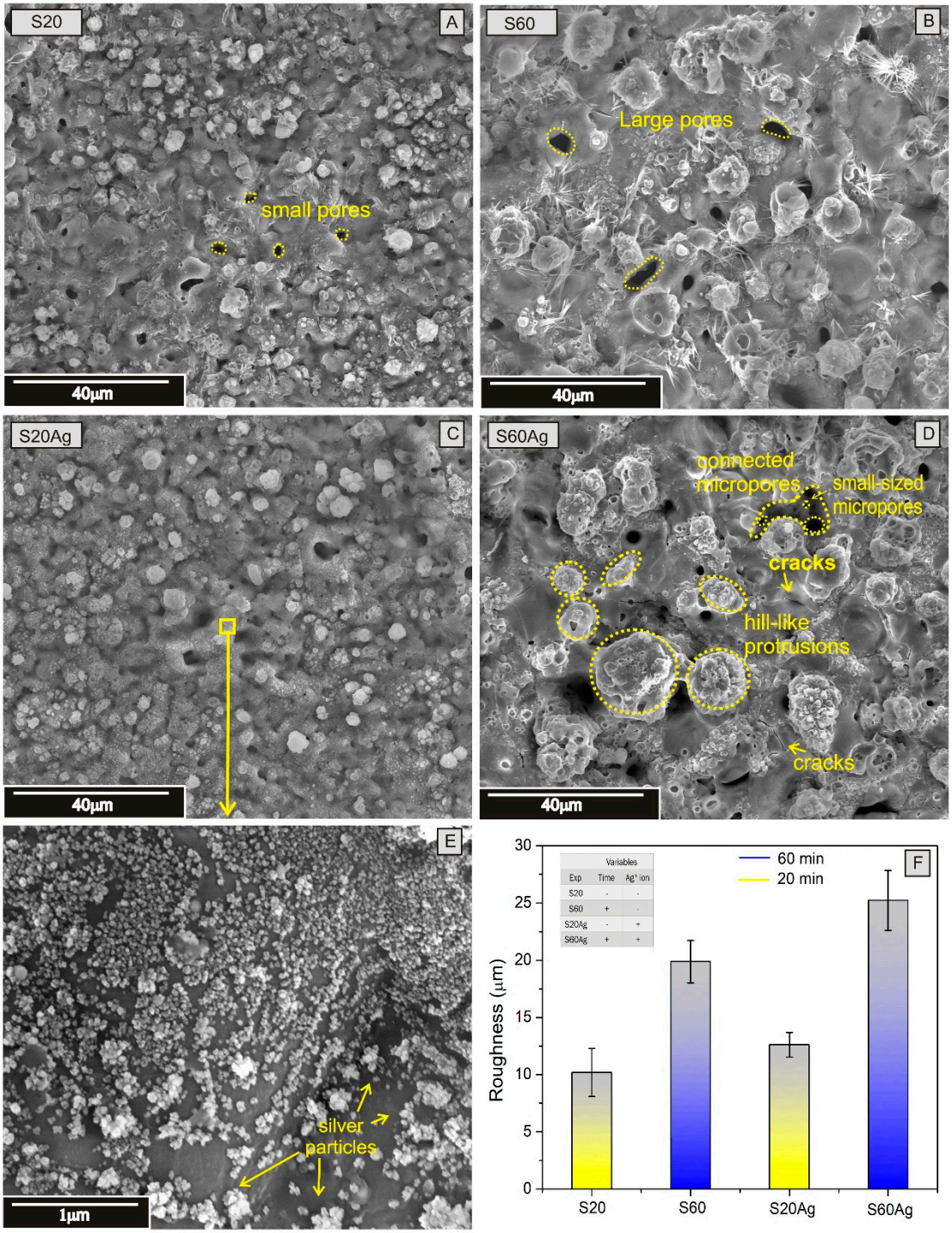

Figure 2. (**A**–**D**) Surface SEM micrographs and (**F**) RMS of anodic oxide coatings obtained using the experimental conditions indicated in Table 1. (**E**) The amplified surface SEM micrograph of the square spot in Figure 2C (the square spot is not in scale).

Furthermore, in SEM micrographs of experiment S60Ag (Figure 2D), where a more compact oxide layer is present, small-sized micropores are observed inside large pores. In addition, morphological aspects have been identified, such as cracks on the surface typically observed in coating produced by the PEO process with an intense discharge regime. The existence of cracks in the oxide surface may be associated with the effect of mechanical stress caused by oxide volume expansion [43] or be a consequence of the PEO dynamic events. Due to this irregular structure, the destructive effects on the film compromised

the estimation of the layer thickness of S60 and S60Ag samples by SEM image analysis. On the other hand, the S20 and S20Ag samples present similar oxide layer thicknesses of 27 ± 1.0 µm.

The different aspects of the morphology shown in SEM micrographs (Figure 2) can be associated with distinct electrical discharge mechanisms as a consequence of the modification of the electrolyte composition during anodization. As mentioned, sparks distributed over the sample at the beginning of anodization present low intensity and a short lifetime. As the anodization continues, the discharges become more intense, concentrated at points, and have longer lifetimes [6,44]. The behavior of electrical discharges during anodization significantly affects the coating morphology [6]. RMS analyses (Figure 2F) reveal that samples anodized for a longer time presented higher roughness (S60 and S60Ag). In addition, the presence of Ag+ ions slightly changed the roughness of the coatings. Erfanifar et al. [45] demonstrated that the surface roughness of oxides produced by PEO increases almost linearly with the thickness of the oxide layer deposited on Al alloys. They suggested that the increase in the roughness was related to increased discharge channel diameter and protrusion height. Other studies have also shown the same behavior on PEO anodization in Al alloys [46–48].

The higher magnification micrograph of experiment S20Ag (Figure 2E) revealed a surface decorated by nanoparticles for a short anodizing time with silver ions in the electrolyte, which was not observed in the samples coated in the other experiments. Therefore, EDS and RBS analyses were carried out to identify the composition of the nanoparticles adhered to the oxide surface. Figure 3 depicts SEM micrographs and the EDS color map of the oxide coating surface for an amplified region of another region of the S20Ag sample. The result revealed that these nanoparticles are composed of silver (blue spots in the color map). Furthermore, the EDS results of all samples (Table 2) showed that the highest percentage of silver (1.01 ± 0.13 at.%) was obtained in the experiment S20Ag.

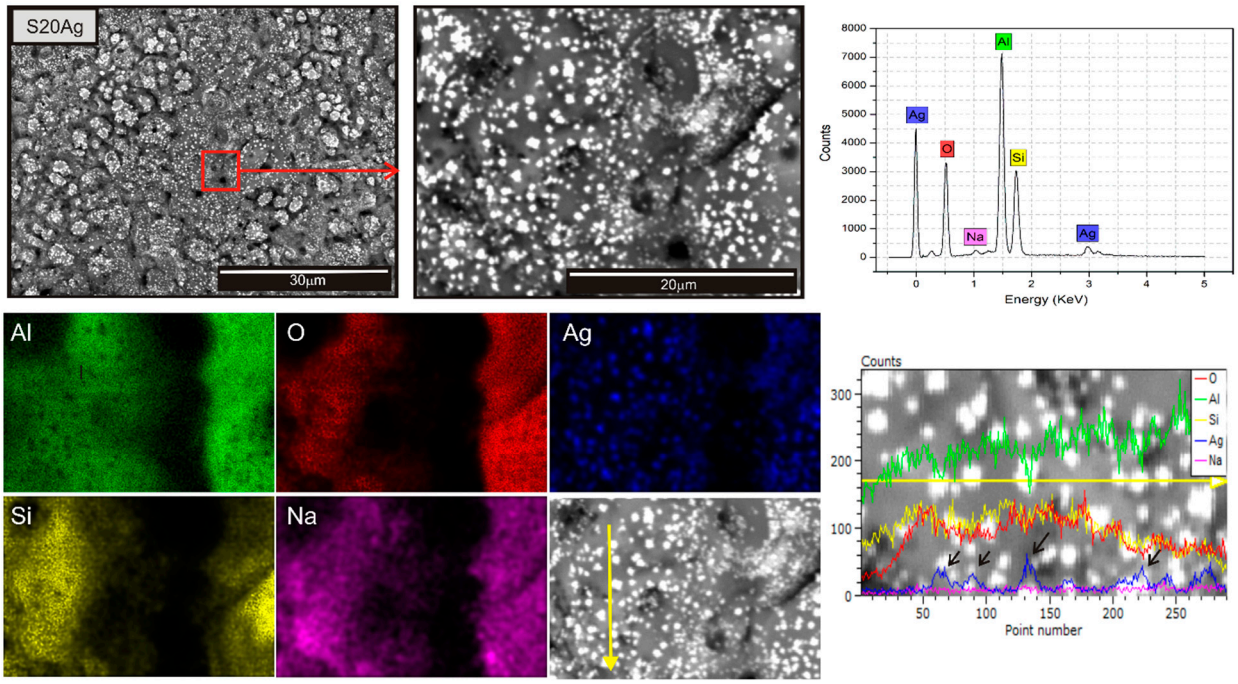

Figure 3. SEM micrographs and elemental analysis obtained by EDS of the PEO coating anodized in 0.1 mol L^{-1} Na_2SiO_3 + 1 mmol L^{-1} $AgNO_3$ for 20 min. The yellow arrow indicates the elemental composition in line. The black arrows indicate the top of the most prominent Ag particles.

Table 2. EDS semi-quantitative analysis of the PEO coating and crystallite size.

Exp.	Al (at.%)	O (at.%)	Si (at.%)	Ag (at.%)	Na (at.%)	N (at.%)	γ-Al_2O_3 Crystallite Size (nm)
S20	28.8 ± 1.2	57.8 ± 0.4	11.1 ± 0.7		1.8 ± 0.1	0.6 ± 0.0	15.1 ± 2.4
S60	17.9 ± 0.3	60.1 ± 0.2	18.9 ± 0.3		2.2 ± 0.2	0.9 ± 0.1	29.4 ± 0.8
S20Ag	27.1 ± 0.7	56.7 ± 0.8	12.8 ± 0.9	1.0 ± 0.1	1.8 ± 0.3	0.6 ± 0.4	14.7 ± 3.1
S60Ag	19.4 ± 0.3	59.9 ± 0.4	18.4 ± 0.2	0.0 ± 0.0	1.5 ± 0.1	0.8 ± 0.2	23.5 ± 3.5

RBS analysis refines the EDS results. The elements O, Na, Al, Si, and Ag are highlighted in the spectra for S20Ag and S60Ag conditions (Figure 4A). For anodization, without Ag ions (S20 e S60), similar spectra (not shown) were obtained, with no counts for silver. Comparing the S20Ag spectrum (red data) with the S60Ag (blue data) clearly shows a good similarity in the number of the major elements and a significant difference in the Ag amount. This difference is quantified in the Ag depth profile for both anodization times (Figure 4B,C), obtained from self-consistent spectra analysis with the MultiSIMNRA platform. In this plot, the thickness of the films is expressed in TFUs, a thickness equivalent unit corresponding to 10^{15} atoms/cm^2. Its use is adequate since RBS does not consider pores [49]. The plot reveals that the Ag atomic concentration is higher at the surface and reduces along the coating. For the anodizing time of 20 min, the self-consist simulation of the spectra suggests that the Ag amount on the surface is a hundred times greater than 60 min of anodization.

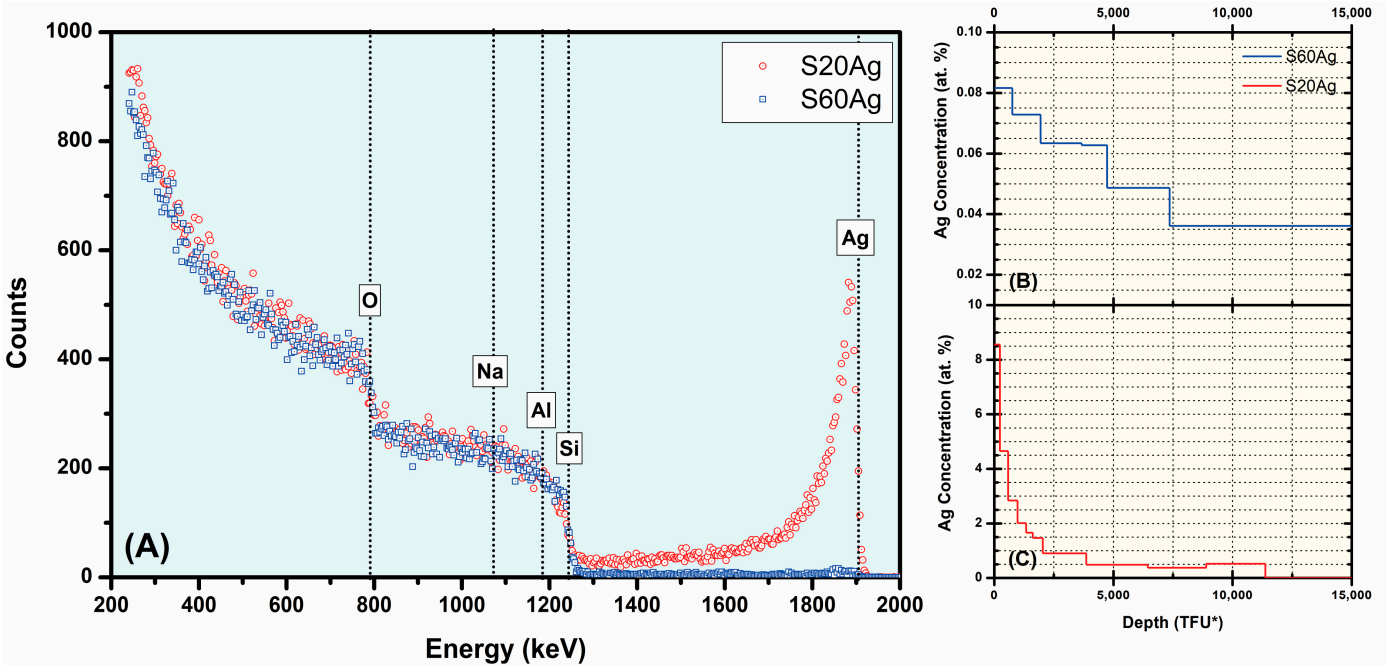

Figure 4. (**A**) RBS spectra of alumina coatings, prepared in different anodization times in the presence of Ag ions in the electrolyte, measured at a scattering angle of 170°. (**B**,**C**) Depth profile of Ag atomic percentage in the coatings from analyses with MultiSIMNRA platform. * TFU are density-independent thickness units, equivalent to mass/area, with TFU ≡ 10^{15} atoms/cm^2.

EDS color map demonstrates strong evidence that the coating produced in the condition of experiment S20Ag contains the elements (Al, O, Si, Na, and Ag) homogeneously distributed over the oxide layer. In addition, however, silver appears as nanoparticle aggregates adhered to the coating surface, as seen in the EDS color map and the SEM micrograph of Figure 3. These results suggest that Ag was deposited at the beginning of the process when a large concentration of Ag^+ ions was available and when the anodic oxide

coating was thinner. This first proposition is based on both prior assumptions regarding the interaction of silicate and Ag^+ ions and the low-intensity spark environment during the beginning of anodization.

A second proposition is based on a simple redox replacement reaction [50,51]. The aluminum presents a negative redox potential ($Al^{3+}/Al = -1.67$ V vs. standard hydrogen electrode (SHE)), and it is well known to be a suitable substrate for manufacturing metallic structures by galvanic displacement. In contrast, Ag presents a positive redox potential ($Ag^+/Ag = +0.8$ V vs. SHE) [50,51]. Therefore, it is feasible to suppose that at the beginning of anodization, when the concentration of Ag+ ions is high, and there is direct contact of these ions to the metallic Al anode, a spontaneous reduction of Ag+ ions over the Al surface might occur [52,53]. EDS analysis also confirms that particles in the nanoscale were metallic Ag (Figure 3). This analysis also confirms that the Ag particles are on the oxide surface following the RBS results since, for the S20Ag samples, the Ag concentration decreases four times in the first three simulated external layers (Figure 4C). The presence of nano aggregates on the coating fits well with the RBS analysis conclusion.

Table 2 describes the semi-quantitative analysis obtained by EDS with the atomic percentage of the elements present in the surface coatings produced by PEO and the crystallite size of the γ-Al_2O_3 phase calculated by the Scherrer equation.

The incorporation of particles and specific chemical elements present in the electrolyte composition is favored in the PEO process because of the dielectric breakdown events that happen simultaneously with plasma ignition [1,6,8,39,54]. The EDS results show a high percentage of oxygen in the coating surfaces, indicating the formation of the Al_2O_3 layer. Furthermore, the Al/Si content (at.%Al/at.%Si) changed from ~2.6 to ~1.0 when the anodization time increased from 20 to 60 min. Some studies also showed that during the PEO of aluminum in a silicate medium, the silicon could be incorporated into the oxide layer in the form of SiO_2 gel layers [38] or mullite ($3Al_2O_3.2SiO_2$) [55]. Nevertheless, this result does not change the effect of the anodization time on the amount of Ag detected over the oxide coating since these silver particles are concentrated in a thinner outer layer of the oxide.

The silver content in the oxide layer was detected only in sample S20Ag considering the EDS results. However, the RBS analysis also detected silver content in sample S20Ag and a small amount of silver in sample S60Ag. Hence, there was a decrease in the silver content percentage in the outer oxide layer during the anodization, indicating that the previously deposited silver nanoparticles could have been dissolved into the electrolyte for an anodization time longer than 20 min. The Ag depth profile from RBS analysis corroborates this (Figure 4B,C). Since the silver concentration for the S60Ag sample is systematically lower along the film thickness, the silver aggregates must have been dissolved in the electrolytic solution during the anodization process. Furthermore, for a more prolonged treatment time, the associated discharge regime changed from a spark to a micro-arc regime [6,56] (Figure 1C,D) when the oxide formation is followed by disruptive events, causing the decrease of the silver previously deposited over the anodic oxide. This result also follows the propositions that consider a reaction between the silver and the silicate ions occurring on the electrolyte side during the anodization.

The high temperature of the electric discharges can crystalize the oxide coatings during the PEO treatment. Figure 5 shows the GIXRD patterns of the PEO coatings prepared according to factorial design conditions described in Table 1.

The peaks of γ-Al_2O_3 were identified in $2\theta = 39.4°$, $45.8°$, $66.9°$ (JCPDS card number 1-1303), and the cubic Al substrate in $2\theta = 38.3°$, $44.8°$, $65°$ and $78°$. (JCPDS card number 4-787) [57]. The crystallization of the oxide coating is spontaneous and occurs due to the dielectric breakdown events [1,54,58]. The intense aluminum peaks revealed that the oxide film is thin enough to expose the metallic substrate. The comparison of the intensities associated with the peak of Al_2O_3 ($2\theta = 66.9°$) and Al ($2\theta = 65°$) showed that for the experiments with 60 min of anodization, there was an Al_2O_3/Al intensity ratio of 0.3, while for the experiments with 20 min of anodization, the intensity ratio was 0.1. This result

tallied with the increase in the crystallite size found for samples produced in a longer anodizing time, which was calculated considering the half-height width of the γ-Al_2O_3 peak, as seen in Table 2.

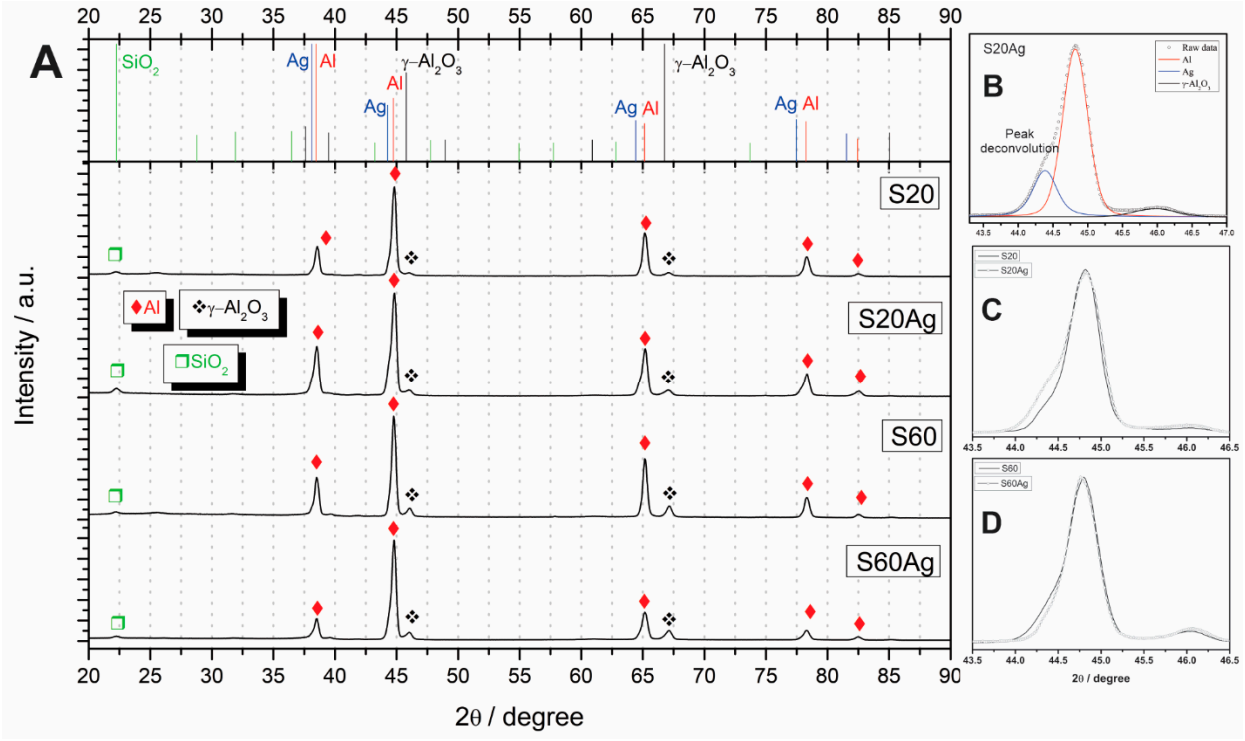

Figure 5. (**A**) X-rays diffractograms for PEO coating of all experiments and the most intensity peaks for Al, Ag, Al_2O_3, and SiO_2 according to JCPDS card numbers 4-787, 4-783, 1-1303, and 82-1406, respectively. (**B**) Deconvolution of peak around 2θ = 44° demonstrating the Ag content. (**C**,**D**) Zoom-in peak 2θ = 44° S20Ag/S20 and S60Ag/S60 samples, respectively.

Regarding the thin outer oxide layer of the coating obtained after 20 min of anodization, Figure 5 shows the most intense peaks expected for the Ag and SiO_2 species since these substances might be present in the first few coating layers, as illustrated in Figure 4B,C, in the RBS depth profile analysis. The silver reflection patterns are almost equivalent to Al reflections. The inset in Figure 5B depicts the deconvolution of peaks around 2θ = 44° in the S20Ag sample. Three deconvoluted peaks can be calculated at 2θ = 44.3°, 2θ = 44.8°, and 2θ = 45.8°, and they can be seen as cubic Ag (JCPDS card number 4-783), cubic Al (JCPDS card number 4-787), and of γ-Al_2O_3. The asymmetry observed in all of the Al reflection peaks' bases might be associated with GIXRD analysis due to the optical configuration of the goniometer and also because we are analyzing solid film samples and not powder. This asymmetry can be better visualized in Figure 5C,D regarding the peaks around 2θ = 44°, which compare samples S20/S20Ag and S60/S60Ag, respectively. Furthermore, a low-intensity peak at 2θ = 22.3° for the most intense hkl peak (101) for the SiO_2 was detected (JCPDS card number 82-1406), indicating the deposition of this species over the anodic oxide coatings.

From the factorial design analysis, the geometric representation in Figure 6 summarizes the results of the microstructural, morphological, and compositional responses when the experimental variables changed from one level (-) to another (+). The vertices of the square represent the values (-) or (+) of each experimental variable studied: anodization time and silver content in the electrolyte, according to the factorial design matrix (Table 1), and the summarized results in Table 2 and Figure 2F. From Figure 6, we can visualize the modification of the corresponding response according to variable values (levels). From the compositional response, an increase in the silicon content (at.%Si) can be observed

when the anodization time increases. As expected, silver was only detected when this element was added to the electrolyte. On the other hand, the roughness and crystallite size increased when the anodization time was increased from 20 min to 60 min. For instance, the roughness of the coatings increased from 10.2 ± 2.1 μm to 25.2 ± 2.5 μm when the anodization time increased, and silver was added to the electrolyte solution.

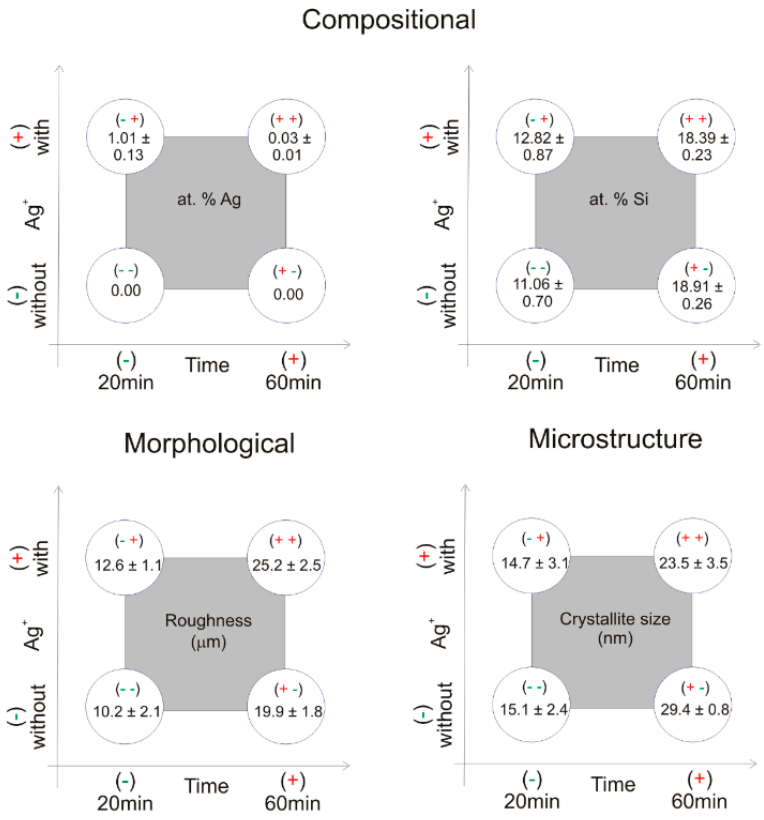

Figure 6. Geometric representation from the analysis of microstructure, morphological, and compositional responses according to the 2^2 factorial design.

Table 3 shows the principal and cross-linked effects of anodization time and the presence of silver on the electrolyte in morphological, microstructural, and compositional responses. The indicated values in bold in Table 3 represent effects with a magnitude higher than the associated error. The results showed that the silver in the electrolyte did not modify the Si content, the crystallite size, or the surface roughness. The exception was observed in the response of silver content (at.%), which was expected since, in this condition, this element was purposely added to the electrolyte. The result from the morphological effect showed that %RMS increased by 11.16 ± 3.15% with anodization time because larger pores and protrusions were obtained in coatings produced in 60 min of anodization treatment, as can be seen in Figure 2. The same behavior was observed in the microstructural response. With the anodization time, the crystallite size of γ-Al_2O_3 crystals increased by 11.55 ± 5.28 nm. This result could be related to the effect of intensification of the electric discharges during the anodization since the electric discharges present high temperatures, creating areas of molten oxide where the crystals can grow [6]. Due to the irregularity and high rugosity of the 60 min samples, it is possible that the grain size may not be homogeneous throughout the oxide layer. In a study performed by Liu et al. [42], the authors showed that the volume of the molten zones changed with anodization time, which can favor the increase in the crystallite size in these regions. Even though the molten oxide regions could be considered an environmental area for the incorporation of impurities from the electrolyte, the crystallite size was influenced by the anodizing time and not by

the presence of silver in the electrolyte because the concentration of $AgNO_3$ is very low (0.001 mol L^{-1}) compared to the silicate anion concentration (0.1 mol L^{-1}).

Table 3. Variable effects on morphological, microstructural, and compositional responses according to 2^2 factorial design.

	Estimative of Variables Effects on Studied Responses			
	Ag Content (at.%)	**Si Content (at.%)**	**γ-Al_2O_3 Crystallite Size (nm)**	**%RMS**
Main Effects ± SD				
Anodizing Time (A)	-0.49 ± 0.14	6.71 ± 1.16	11.55 ± 5.28	11.16 ± 3.15
Ag^+ ion (B)	0.52 ± 0.14	0.62 ± 1.16	-3.15 ± 5.28	3.89 ± 3.15
Interaction of two factors ± SD				
A × B	-0.49 ± 0.14	-1.15 ± 1.16	-2.75 ± 5.28	1.46 ± 3.15

The cross-linked interaction from both variables (anodization time and presence of silver in the electrolyte) indicates a decrease in the Ag content, indicating that both variables, when changing simultaneously during the anodization caused a decrease by -0.49 ± 0.14 at.% in that element content in the produced anodic coating. The other effects in Table 3 that presented lower values than the associated errors are not statistically significant and can be disregarded.

To summarize, the most critical variable in the factorial design analysis was the anodization time, which significantly modifies all responses, particularly the Ag content (at.%) as nanoparticles adhered over the coating surface.

4. Conclusions

This study explored the effects of adding silver ions in the electrolyte used to produce PEO coatings on commercial aluminum. A factorial design was used to verify the effects of the variables' "anodization time" and the "presence of silver" on the compositional, morphological, and microstructural responses. The deposition of this element in the anodic oxide coating was achieved by adding this element in ionic form into the electrolyte in a fast-one-step synthesis of the PEO process. The PEO process promoted the oxide crystallization, producing a thin layer of γ-Al_2O_3 over the Al substrate. SEM micrographs of different samples showed that the main features of the coating's morphology were not modified by silver particles on the electrolyte, displaying a typical structure with irregular porous and protrusions on the surface produced by PEO under the DC regime. EDS and RBS analysis depicted that the coating composition is formed mainly by aluminum and silicon oxides. For one specific condition, a higher silver percentage was homogeneously deposited on the oxide surface in the form of several dispersed silver nanoparticles. From the factorial design analysis, the increase in the anodization time caused an increase in the roughness, γ-Al_2O_3 crystallite size, and Si content in the coating. On the other hand, increasing the anodization time decreased the Ag content but increased the surface roughness of all samples. The sample produced in 20 min exhibited significant content of silver than the sample anodized in 60 min.

Author Contributions: Conceptualization, F.T.-S., J.S.S. and M.S.S.; Methodology, M.S.S.; Software, J.S.S.; Formal analysis, F.T.-S. and J.S.S.; Investigation, F.T.-S., A.O.D.-S., J.S.S., A.R., G.P.M. and M.S.S.; Writing—original draft, F.T.-S., A.O.D.-S., J.S.S. and A.R.; Writing—review & editing, F.T.-S., J.S.S. and M.S.S.; Supervision, F.T.-S.; Project administration, F.T.-S.; Funding acquisition, F.T.-S. All authors have read and agreed to the published version of the manuscript.

Funding: This research was funded by Brazilian Research Funding Agencies FAPESP (grant number 2022/05195-3), CNPq (grant number 443125/2014-7, grant number 135736/2015-3 and grant number 408250/2016-0), and CAPES (grant number PNPD20131497 and financial code 01).

Data Availability Statement: Scientific data are available upon request directly from the corresponding author.

Acknowledgments: The authors are grateful to CNPEM-LNNano, which provided an opening shift for using FEG-SEM Quanta with EDS that allowed high-resolution characterizations and LAMFI (USP) for the RBS measurements.

Conflicts of Interest: The authors declare no conflict of interest.

References

1. Clyne, T.W.; Troughton, S.C. A review of recent work on discharge characteristics during plasma electrolytic oxidation of various metals. *Int. Mater. Rev.* **2019**, *64*, 127–162. [CrossRef]
2. Babaei, K.; Fattah-alhosseini, A.; Chaharmahali, R. A review on plasma electrolytic oxidation (PEO) of niobium: Mechanism, properties and applications. *Surf. Interfaces* **2020**, *21*, 100719. [CrossRef]
3. Trivinho-Strixino, F.; Santos, J.S.; Souza Sikora, M. 3-Electrochemical Synthesis of Nanostructured Materials. In *Nanostructures*; Da Róz, A.L., Ferreira, M., de Lima Leite, F., Oliveira, O.N., Eds.; William Andrew Publishing: Norwich, NY, USA, 2017.
4. Santos, J.S.; Trivinho-Strixino, F.; Pereira, E.C. The influence of experimental conditions on the morphology and phase composition of Nb-doped ZrO_2 films prepared by spark anodization. *Corros. Sci.* **2013**, *73*, 99–105. [CrossRef]
5. Trivinho-Strixino, F.; Silva, D.X.; Paiva-Santos, C.O.; Pereira, E.C. Tetragonal to monoclinic phase transition observed during Zr anodisation. *J. Solid State Electrochem.* **2013**, *17*, 191–199. [CrossRef]
6. Santos, J.S.; Lemos, S.G.; Gonçalves, W.N.; Bruno, O.M.; Pereira, E.C. Characterization of electrical discharges during spark anodization of zirconium in different electrolytes. *Electrochim. Acta* **2014**, *130*, 477–487. [CrossRef]
7. Sikora, M.S.; Carstensen, J.; Föll, H.; Pereira, E.C. Theoretical Calculation of the Local Heating Effect on the Crystallization of TiO_2 Prepared by Sparking Anodization. *Curr. Nanosci.* **2015**, *11*, 263–270. [CrossRef]
8. Lu, X.; Mohedano, M.; Blawert, C.; Matykina, E.; Arrabal, R.; Kainer, K.U.; Zheludkevich, M.L. Plasma electrolytic oxidation coatings with particle additions—A review. *Surf. Coat. Technol.* **2016**, *307* (Pt. C), 1165–1182. [CrossRef]
9. Lu, X.; Blawert, C.; Zheludkevich, M.L.; Kainer, K.U. Insights into plasma electrolytic oxidation treatment with particle addition. *Corros. Sci.* **2015**, *101*, 201–207. [CrossRef]
10. Trivinho-Strixino, F.; Guimaraes, F.E.G.; Pereira, E.C. Luminescence in anodic ZrO_2 doped with Eu(III)ions. *Mol. Cryst. Liq. Cryst.* **2008**, *485*, 766–775. [CrossRef]
11. Orsetti, F.R.; Bukman, L.; Santos, J.S.; Nagay, B.E.; Rangel, E.C.; Cruz, N.C. Methylene blue and metformin photocatalytic activity of CeO_2-Nb_2O_5 coatings is dependent on the treatment time of plasma electrolytic oxidation on titanium. *Appl. Surf. Sci. Adv.* **2021**, *6*, 100143. [CrossRef]
12. Babaei, K.; Fattah-alhosseini, A.; Molaei, M. The effects of carbon-based additives on corrosion and wear properties of Plasma electrolytic oxidation (PEO) coatings applied on Aluminum and its alloys: A review. *Surf. Interfaces* **2020**, *21*, 100677. [CrossRef]
13. Liu, W.; Pu, Y.; Liao, H.; Lin, Y.; He, W. Corrosion and Wear Behavior of PEO Coatings on D16T Aluminum Alloy with Different Concentrations of Graphene. *Coatings* **2020**, *10*, 249. [CrossRef]
14. Arrabal, R.; Mohedano, M.; Matykina, E.; Pardo, A.; Mingo, B.; Merino, M.C. Characterization and wear behaviour of PEO coatings on 6082-T6 aluminium alloy with incorporated α-Al_2O_3 particles. *Surf. Coat. Technol.* **2015**, *269*, 64–73. [CrossRef]
15. Hu, C.-J.; Hsieh, M.-H. Preparation of ceramic coatings on an Al–Si alloy by the incorporation of ZrO_2 particles in microarc oxidation. *Surf. Coat. Technol.* **2014**, *258*, 275–283. [CrossRef]
16. Rudnev, V.S.; Lukiyanchuk, I.V.; Vasilyeva, M.S.; Morozova, V.P.; Zelikman, V.M.; Tarkhanova, I.G. W-containing oxide layers obtained on aluminum and titanium by PEO as catalysts in thiophene oxidation. *Appl. Surf. Sci.* **2017**, *422*, 1007–1014. [CrossRef]
17. Tyrina, L.M.; Rudnev, V.S.; Lukiyanchuk, I.V.; Ustinov, A.Y.; Sergienko, V.I.; Vasil'eva, M.S.; Kondrikov, N.B. Ni- and Cu-containing oxide layers on aluminum: Formation, composition, and catalytic properties. *Dokl. Phys. Chem.* **2007**, *415*, 183–185. [CrossRef]
18. Tyrina, L.M.; Rudnev, V.S.; Nedozorov, P.M.; Ustiniov, A.Y.; Lukiyanchuk, I.V.; Kaidalova, T.A. Preparation, properties, and catalytic activity of platinum-modified plasma electrolytic oxide structures on aluminum. *Russ. J. Inorg. Chem.* **2011**, *56*, 1429. [CrossRef]
19. Jin, F.; Tong, H.; Li, J.; Shen, L.; Chu, P.K. Structure and microwave-absorbing properties of Fe-particle containing alumina prepared by micro-arc discharge oxidation. *Surf. Coat. Technol.* **2006**, *201*, 292–295. [CrossRef]
20. Rogov, A.B.; Terleeva, O.P.; Mironov, I.V.; Slonova, A.I. Iron-containing coatings obtained by microplasma method on aluminum with usage of homogeneous electrolytes. *Appl. Surf. Sci.* **2012**, *258*, 2761–2765. [CrossRef]
21. Cerchier, P.; Pezzato, L.; Gennari, C.; Moschin, E.; Moro, I.; Dabalà, M. PEO coating containing copper: A promising anticorrosive and antifouling coating for seawater application of AA 7075. *Surf. Coat. Technol.* **2020**, *393*, 125774. [CrossRef]
22. Cerchier, P.; Pezzato, L.; Moschin, E.; Coelho, L.B.; Olivier, M.G.M.; Moro, I.; Magrini, M. Antifouling properties of different Plasma Electrolytic Oxidation coatings on 7075 aluminium alloy. *Int. Biodeterior. Biodegrad.* **2018**, *133*, 70–78. [CrossRef]
23. Cerchier, P.; Pezzato, L.; Brunelli, K.; Dolcet, P.; Bartolozzi, A.; Bertani, R.; Dabalà, M. Antibacterial effect of PEO coating with silver on AA7075. *Mater. Sci. Eng. C* **2017**, *75*, 554–564. [CrossRef] [PubMed]
24. Pezzato, L.; Cerchier, P.; Brunelli, K.; Bartolozzi, A.; Bertani, R.; Dabalà, M. Plasma electrolytic oxidation coatings with fungicidal properties. *Surf. Eng.* **2019**, *35*, 325–333. [CrossRef]

25. Santos, J.S.; Rodrigues, A.; Simon, A.P.; Ferreira, C.H.; Santos, V.A.Q.; Sikora, M.S.; Cruz, N.C.; Mambrini, G.P.; Trivinho-Strixino, F. One-Step Synthesis of Antibacterial Coatings by Plasma Electrolytic Oxidation of Aluminum. *Adv. Eng. Mater.* **2019**, *21*, 1900119. [CrossRef]
26. Santos, J.S.; Márquez, V.; Buijnsters, J.G.; Praserthdam, S.; Praserthdam, P. Antimicrobial properties dependence on the composition and architecture of copper-alumina coatings prepared by plasma electrolytic oxidation (PEO). *Appl. Surf. Sci.* **2023**, *607*, 155072. [CrossRef]
27. Thukkaram, M.; Cools, P.; Nikiforov, A.; Rigole, P.; Coenye, T.; Van Der Voort, P.; Du Laing, G.; Vercruysse, C.; Declercq, H.; Morent, R.; et al. Antibacterial activity of a porous silver doped TiO_2 coating on titanium substrates synthesized by plasma electrolytic oxidation. *Appl. Surf. Sci.* **2020**, *500*, 144235. [CrossRef]
28. Rizwan, M.; Alias, R.; Zaidi, U.Z.; Mahmoodian, R.; Hamdi, M. Surface modification of valve metals using plasma electrolytic oxidation for antibacterial applications: A review. *J. Biomed. Mater. Res. Part A* **2018**, *106*, 590–605. [CrossRef]
29. Zhu, W.; Zhang, Z.; Gu, B.; Sun, J.; Zhu, L. Biological Activity and Antibacterial Property of Nano-structured TiO_2 Coating Incorporated with Cu Prepared by Micro-arc Oxidation. *J. Mater. Sci. Technol.* **2013**, *29*, 237–244. [CrossRef]
30. Zhang, D.; Han, Q.; Yu, K.; Lu, X.; Liu, Y.; Lu, Z.; Wang, Q. Antibacterial activities against Porphyromonas gingivalis and biological characteristics of copper-bearing PEO coatings on magnesium. *J. Mater. Sci. Technol.* **2021**, *61*, 33–45. [CrossRef]
31. Necula, B.S.; Fratila-Apachitei, L.E.; Zaat, S.A.J.; Apachitei, I.; Duszczyk, J. In vitro antibacterial activity of porous TiO_2–Ag composite layers against methicillin-resistant Staphylococcus aureus. *Acta Biomater.* **2009**, *5*, 3573–3580. [CrossRef]
32. Muhaffel, F.; Cimenoglu, H. Development of corrosion and wear resistant micro-arc oxidation coating on a magnesium alloy. *Surf. Coat. Technol.* **2019**, *357*, 822–832. [CrossRef]
33. Dancer, S.J. How Much Impact Do Antimicrobial Surfaces Really Have on Healthcare-acquired Infection? *Clin. Infect. Dis.* **2020**, *71*, 1814–1816. [CrossRef] [PubMed]
34. Ellingson, K.D.; Pogreba-Brown, K.; Gerba, C.P.; Elliott, S.P. Impact of a Novel Antimicrobial Surface Coating on Health Care-Associated Infections and Environmental Bioburden at 2 Urban Hospitals. *Clin. Infect. Dis. Off. Publ. Infect. Dis. Soc. Am.* **2020**, *71*, 1807–1813. [CrossRef] [PubMed]
35. Silva, T.F.; Rodrigues, C.L.; Mayer, M.; Moro, M.V.; Trindade, G.F.; Aguirre, F.R.; Added, N.; Rizzutto, M.A.; Tabacniks, M.H. MultiSIMNRA: A computational tool for self-consistent ion beam analysis using SIMNRA. *Nucl. Instrum. Methods Phys. Res. Sect. B Beam Interact. Mater. At.* **2016**, *371*, 86–89. [CrossRef]
36. Mayer, M. SIMNRA, a simulation program for the analysis of NRA, RBS and ERDA. *AIP Conf. Proc.* **1999**, *475*, 541–544. [CrossRef]
37. Rashad, M.M.; Baioumy, H.M. Effect of thermal treatment on the crystal structure and morphology of zirconia nanopowders produced by three different routes. *J. Mater. Process. Technol.* **2008**, *195*, 178–185. [CrossRef]
38. Monfort, F.; Berkani, A.; Matykina, E.; Skeldon, P.; Thompson, G.E.; Habazaki, H.; Shimizu, K. Development of anodic coatings on aluminium under sparking conditions in silicate electrolyte. *Corros. Sci.* **2007**, *49*, 672–693. [CrossRef]
39. Parkhutik, V.P.; Albella, J.M.; Martinez-Duart, J.M. Electric Breakdown in Anodic Oxide Films. In *Moderns Aspects of Electrochemistry*; Bockris, J.O.M., Conway, B.E., White, R.E., Eds.; Plenum Press: New York, NY, USA, 1992; Volume 23.
40. Ikonopisov, S.; Girginov, A.; Machkova, M. Electrical breaking down of barrier anodic films during their formation. *Electrochim. Acta* **1979**, *24*, 451–456. [CrossRef]
41. Liu, X.; Wang, S.; Du, N.; Li, X.; Zhao, Q. Evolution of the Three-Dimensional Structure and Growth Model of Plasma Electrolytic Oxidation Coatings on 1060 Aluminum Alloy. *Coatings* **2018**, *8*, 105. [CrossRef]
42. Di Quarto, F.; Piazza, S.; Sunseri, C. A phenomenological approach to the mechanical breakdown of anodic oxide films on zirconium. *Corros. Sci.* **1986**, *26*, 213–221. [CrossRef]
43. Hussein, R.O.; Nie, X.; Northwood, D.O.; Yerokhin, A.; Matthews, A. Spectroscopic study of electrolytic plasma and discharging behaviour during the plasma electrolytic oxidation (PEO) process. *J. Phys. D Appl. Phys.* **2010**, *43*, 105203. [CrossRef]
44. Erfanifar, E.; Aliofkhazraei, M.; Fakhr Nabavi, H.; Sharifi, H.; Rouhaghdam, A.S. Growth kinetics and morphology of plasma electrolytic oxidation coating on aluminum. *Mater. Chem. Phys.* **2017**, *185*, 162–175. [CrossRef]
45. Tian, J.; Luo, Z.; Qi, S.; Sun, X. Structure and antiwear behavior of micro-arc oxidized coatings on aluminum alloy. *Surf. Coat. Technol.* **2002**, *154*, 1–7. [CrossRef]
46. Sundararajan, G.; Rama Krishna, L. Mechanisms underlying the formation of thick alumina coatings through the MAO coating technology. *Surf. Coat. Technol.* **2003**, *167*, 269–277. [CrossRef]
47. Wang, L.; Nie, X. Silicon effects on formation of EPO oxide coatings on aluminum alloys. *Thin Solid Film.* **2006**, *494*, 211–218. [CrossRef]
48. Mohapatra, P.; Shaw, S.; Mendivelso-Perez, D.; Bobbitt, J.M.; Silva, T.F.; Naab, F.; Yuan, B.; Tian, X.; Smith, E.A.; Cademartiri, L. Calcination does not remove all carbon from colloidal nanocrystal assemblies. *Nat. Commun.* **2017**, *8*, 2038. [CrossRef]
49. Rafailovic, L.; Gammer, C.; Rentenberger, C.; Trišović, T.; Kleber, C.; Peter Karnthaler, H. Functionalizing Aluminum Oxide by Ag Dendrite Deposition at the Anode during Simultaneous Electrochemical Oxidation of Al. *Adv. Mater.* **2015**, *27*, 6438–6443. [CrossRef]
50. Fu, J.; Ye, W.; Wang, C. Facile Synthesis of Ag Dendrites on Al Foil via Galvanic Replacement Reaction with $[Ag(NH_3)_2]Cl$ for Ultrasensitive SERS Detecting of Biomolecules. *Mater. Chem. Phys.* **2013**, *141*, 107–113. [CrossRef]
51. Eliaz, N.; Gileadi, E. *Physical Electrochemistry: Fundamentals, Techniques, and Applications*; Wiley: Hoboken, NJ, USA, 2018.
52. Crow, D.R. *Principles and Applications of Electrochemistry*; CRC Press: Boca Raton, FL, USA, 2017.

53. Dunleavy, C.S.; Golosnoy, I.O.; Curran, J.A.; Clyne, T.W. Characterisation of discharge events during plasma electrolytic oxidation. *Surf. Coat. Technol.* **2009**, *203*, 3410–3419. [CrossRef]
54. Lv, G.; Gu, W.; Chen, H.; Feng, W.; Khosa, M.L.; Li, L.; Niu, E.; Zhang, G.; Yang, S.-Z. Characteristic of ceramic coatings on aluminum by plasma electrolytic oxidation in silicate and phosphate electrolyte. *Appl. Surf. Sci.* **2006**, *253*, 2947–2952. [CrossRef]
55. Matykina, E.; Monfort, F.; Berkani, A.; Skeldon, P.; Thompson, G.E.; Gough, J. Characterization of Spark-Anodized Titanium for Biomedical Applications. *J. Electrochem. Soc.* **2007**, *154*, C279–C285. [CrossRef]
56. McMurdie, H.F.; Morris, M.C.; Evans, E.H.; Paretzkin, B.; Wong-Ng, W.; Hubbard, C.R. Standard X-ray Diffraction Powder Patterns from The JCPDS Research Associateship. *Powder Diffr.* **2013**, *1*, 265–275. [CrossRef]
57. Matykina, E.; Arrabal, R.; Pardo, A.; Mohedano, M.; Mingo, B.; Rodríguez, I.; González, J. Energy-efficient PEO process of aluminium alloys. *Mater. Lett.* **2014**, *127*, 13–16. [CrossRef]
58. Neufeld, P.; Nagpaul, N.K.; Ashdown, R.; Akbar, M. Crystallization of anodic Al_2O_3. *Electrochim. Acta* **1972**, *17*, 1543–1546. [CrossRef]